PLB-985 Neutrophil-Like Cells as a Model To Study *Aspergillus fumigatus* Pathogenesis

Muhammad Rafiq,[a,b] Flora Rivieccio,[a,b] Ann-Kathrin Zimmermann,[a,b] Corissa Visser,[a,b] Alexander Bruch,[c] Thomas Krüger,[a] Katherine González Rojas,[a,b] Olaf Kniemeyer,[a,b] Matthew G. Blango,[c] Axel A. Brakhage[a,b]

[a]Department of Molecular and Applied Microbiology, Leibniz Institute for Natural Product Research and Infection Biology - Hans Knöll Institute (Leibniz-HKI), Jena, Germany

[b]Department of Microbiology and Molecular Biology, Institute of Microbiology, Friedrich Schiller University, Jena, Germany

[c]Junior Research Group RNA Biology of Fungal Infections, Leibniz Institute for Natural Product Research and Infection Biology - Hans Knöll Institute (Leibniz-HKI), Jena, Germany

Muhammad Rafiq, Flora Rivieccio, and Ann-Kathrin Zimmermann contributed equally to the manuscript and are listed alphabetically.

ABSTRACT Fungal infections remain a major global concern. Emerging fungal pathogens and increasing rates of resistance mean that additional research efforts and resources must be allocated to advancing our understanding of fungal pathogenesis and developing new therapeutic interventions. Neutrophilic granulocytes are a major cell type involved in protection against the important fungal pathogen *Aspergillus fumigatus*, where they employ numerous defense mechanisms, including production of antimicrobial extracellular vesicles. A major drawback to work with neutrophils is the lack of a suitable cell line system for the study of fungal pathogenesis. To address this problem, we assessed the feasibility of using differentiated PLB-985 neutrophil-like cells as an *in vitro* model to study *A. fumigatus* infection. We find that dimethylformamide-differentiated PLB-985 cells provide a useful recapitulation of many aspects of *A. fumigatus* interactions with primary human polymorphonuclear leukocytes. We show that differentiated PLB-985 cells phagocytose fungal conidia and acidify conidia-containing phagolysosomes similar to primary neutrophils, release neutrophil extracellular traps, and also produce antifungal extracellular vesicles in response to infection. In addition, we provide an improved method for the isolation of extracellular vesicles produced during infection by employing a size exclusion chromatography-based approach. Advanced liquid chromatography-tandem mass spectrometry (LC-MS/MS) proteomics revealed an enrichment of extracellular vesicle marker proteins and a decrease of cytoplasmic proteins in extracellular vesicles isolated using this improved method. Ultimately, we find that differentiated PLB-985 cells can serve as a genetically tractable model to study many aspects of *A. fumigatus* pathogenesis.

IMPORTANCE Polymorphonuclear leukocytes are an important defense against human fungal pathogens, yet our model systems to study this group of cells remain very limited in scope. In this study, we established that differentiated PLB-985 cells can serve as a model to recapitulate several important aspects of human polymorphonuclear leukocyte interactions with the important human fungal pathogen *Aspergillus fumigatus*. The proposed addition of a cultured neutrophil-like cell line to the experimental toolbox to study fungal pathogenesis will allow for a more mechanistic description of neutrophil antifungal biology. In addition, the easier handling of the cell line compared to primary human neutrophils allowed us to use PLB-985 cells to provide an improved method for isolation of neutrophil-derived extracellular vesicles using size exclusion chromatography. Together, these results provide significant tools and a baseline knowledge for the future study of neutrophil-derived extracellular vesicles in the laboratory.

Fungal infections remain a tremendous source of global morbidity and mortality. More than 1 billion individuals are affected per year, with invasive infections killing numbers comparable to other leading bacterial pathogens (>1.5 million per year [gaffi.org] [1]). Deadly invasive infections are caused by a relatively small number of fungi, with most of these attributed to members of the genera *Candida*, *Pneumocystis*, *Cryptococcus*, and *Aspergillus* (2). *Aspergillus fumigatus* is the major cause of aspergillosis and is particularly dangerous to immunocompromised individuals suffering from neutropenia (3). There is also emerging evidence to suggest that invasive aspergillosis may contribute to coronavirus disease 2019 (COVID-19)-related deaths (4, 5), but challenges in safely obtaining bronchoalveolar lavage samples from these patients have often made confirmatory diagnosis difficult. Despite the obvious importance of *A. fumigatus* in the clinic, our understanding of this important pathogen remains lacking in many aspects, in part due to a lack of tractable experimental systems in the laboratory.

Mammals are continuously challenged by fungal pathogens. In fact, asexual spores of *A. fumigatus*, termed conidia, are thought to be inhaled by humans on a scale of hundreds per day (6). For most fungi, the body temperature of mammals is too high to allow for growth, but for organisms like *A. fumigatus* that thrive in compost piles at high temperatures, the human host provides fertile ground in the absence of a functional immune system (7). However, humans do have multiple additional defenses, including a mucociliary escalator to remove particles from the lungs, a robust epithelium, resident alveolar macrophages that eliminate the majority of the remaining fungal conidia, and infiltrating polymorphonuclear leukocytes (PMNs) that aid in clearance of conidia and destruction of fungal hyphae, among others (3, 8). Neutrophils play an essential role in antifungal defense, due to their importance in killing fungal hyphae. This is well illustrated by the high susceptibility of neutropenic patients to *A. fumigatus* infections in clinics (reviewed in references 3 and 9).

Studies of primary human neutrophils have revealed the capacity of these cells to phagocytose conidia and release granules, neutrophil extracellular traps (NETs), and extracellular vesicles in response to invading pathogens (10–12). Phagocytosis occurs in conjunction with recognition of pathogen-associated molecular patterns by host pathogen recognition receptors. Studies of zebrafish and mice have shown that these internalized conidia can even be passed from neutrophils to macrophages for destruction of the fungus (13), implying complex intracellular trafficking. In neutrophils and macrophages however, internalized wild-type *A. fumigatus* conidia are capable of stalling phagolysosomal acidification to facilitate outgrowth (14).

In addition to phagocytosis, NETs are an important mechanism of defense against *A. fumigatus* that are produced in response to fungal recognition in a CD11b-dependent manner (11, 15). NET production is most abundant against hyphae, but NETs are also sometimes produced in response to resting and swollen conidia (16). *In vivo*, NETs were shown to be present in mouse lungs during infection but were generally dispensable for fungal clearance (16, 17), suggesting that alternative measures are required to eliminate fungal hyphae that escaped phagocytosis as conidia.

Neutrophilic granules and extracellular vesicles are two heterogeneous subcellular populations that also contribute widely to the antimicrobial response. Proteins associated with granules like lactoferrin are known to inhibit *A. fumigatus* conidial germination due to iron sequestration (18), and the abundant granule protein myeloperoxidase inhibits fungal hyphal growth (19). Extracellular vesicles were also shown to provide an antifungal mechanism against *A. fumigatus* hyphae and conidia (10). Antifungal extracellular vesicles produced by neutrophils in response to infection are capable of associating with the fungal cell wall and are in some cases internalized to deliver an unknown antifungal cargo. Intriguingly, the antifungal effect of these extracellular vesicles appeared to be tailored to the infecting pathogen, as spontaneously released

vesicles and vesicles released in response to infection with a knockout strain deficient in production of the conidial pigment dihydroxynaphthalene (DHN)-melanin were not antifungal against wild-type fungus (10).

The molecular mechanisms behind these differences in antifungal potential are difficult to discern in the absence of a tractable model system for the genetic manipulation of neutrophils. Despite the importance of neutrophils in antifungal defense, the majority of studies are still performed in primary human PMNs isolated from venous blood, a resource that can be used only for small-scale studies and is unfortunately highly variable between blood donors. A laborious isolation procedure and limited half-life of about 19 h *ex vivo* (20) also make more mechanistic studies difficult. For these reasons, establishment of a cell culture line to study *A. fumigatus* pathogenesis in neutrophils or neutrophil-like cells would be highly advantageous. In recent years, some options to investigate specific aspects of neutrophil biology in culture have emerged (21). In particular, the myeloid cell line PLB-985, a derivative of HL-60 granulocytic cells, seems a tractable model to study NET formation in response to bacterial infection after differentiation into neutrophil-like cells (22, 23). Of note, the related HL-60 cell line has also been used to deliver azole drugs to *A. fumigatus*-infected mice (24), but not to our knowledge in studies of *A. fumigatus* pathogenesis.

Here, we hypothesized that differentiated human PLB-985 neutrophil-like cells could serve as a model system to study the host pathogenesis of *A. fumigatus* in a blood donor-independent manner. We tested this hypothesis by defining the phagocytosis and intracellular trafficking of *A. fumigatus* conidia by PLB-985 cells, the production of neutrophil extracellular traps, and the release of extracellular vesicles produced in response to fungal infection. We find numerous similarities between this cell line and primary neutrophils that suggest differentiated PLB-985 cells can serve as a tractable *in vitro* model system for further study of some aspects of *A. fumigatus* pathogenesis.

RESULTS

Differentiated PLB-985 neutrophil-like cells phagocytose opsonized *A. fumigatus* conidia. We set out to assess the feasibility of using *N,N*-dimethylformamide (DMF)-differentiated PLB-985 (dPLB) cells as a model for neutrophil phagocytosis, NET production, and extracellular vesicle release in response to *A. fumigatus* infection. Upon infection, neutrophils are known to rapidly phagocytose and process *A. fumigatus* conidia. We therefore challenged dPLB cells with opsonized *A. fumigatus* resting conidia and assessed various parameters of infection.

First, we determined the phagocytic capacity of PLB-985 cells using confocal laser scanning microscopy following incubation of cells with fluorescein isothiocyanate (FITC)-labeled, opsonized conidia (green). We observed that dPLBs were capable of phagocytosis, as evidenced by a phagosomal membrane surrounding the conidia (Fig. 1A). A similar result was confirmed for primary human PMNs with this experimental setup (see Fig. S1A in the supplemental material). The dPLB cells only infrequently phagocytosed unopsonized conidia, highlighting the importance of opsonization and consistent with previous findings in primary human neutrophils (25). To better quantify phagocytosis, we analyzed 5,000 host cells postinfection with opsonized conidia by single-cell analysis using imaging flow cytometry. To do this, we counterstained with calcofluor white (CFW; blue) to elucidate nonphagocytosed conidia (Fig. 1B and Fig. S1B and S1C). Quantification revealed that approximately 22% of wild-type and 26% of nonpigmented Δ*pksP* conidia were phagocytosed by dPLBs after 2 h, while undifferentiated PLB-985 cells exhibited limited phagocytosis of both wild-type and nonpigmented conidia (Fig. 1C). As expected, these phagocytosis percentages were lower than those of primary human PMNs, which aggressively phagocytosed conidia (Fig. S1D). To determine whether infection also resulted in an activated immune response, we measured proinflammatory cytokine levels by an enzyme-linked immunosorbent assay (ELISA). Coincubation of dPLB cells with wild-type spores resulted in production of significantly increased levels of interleukin 8 (IL-8), but not IL-1β after 24 h of coincubation, comparable to time points with primary human PMNs (Fig. 1D and Fig. S2). Together, these
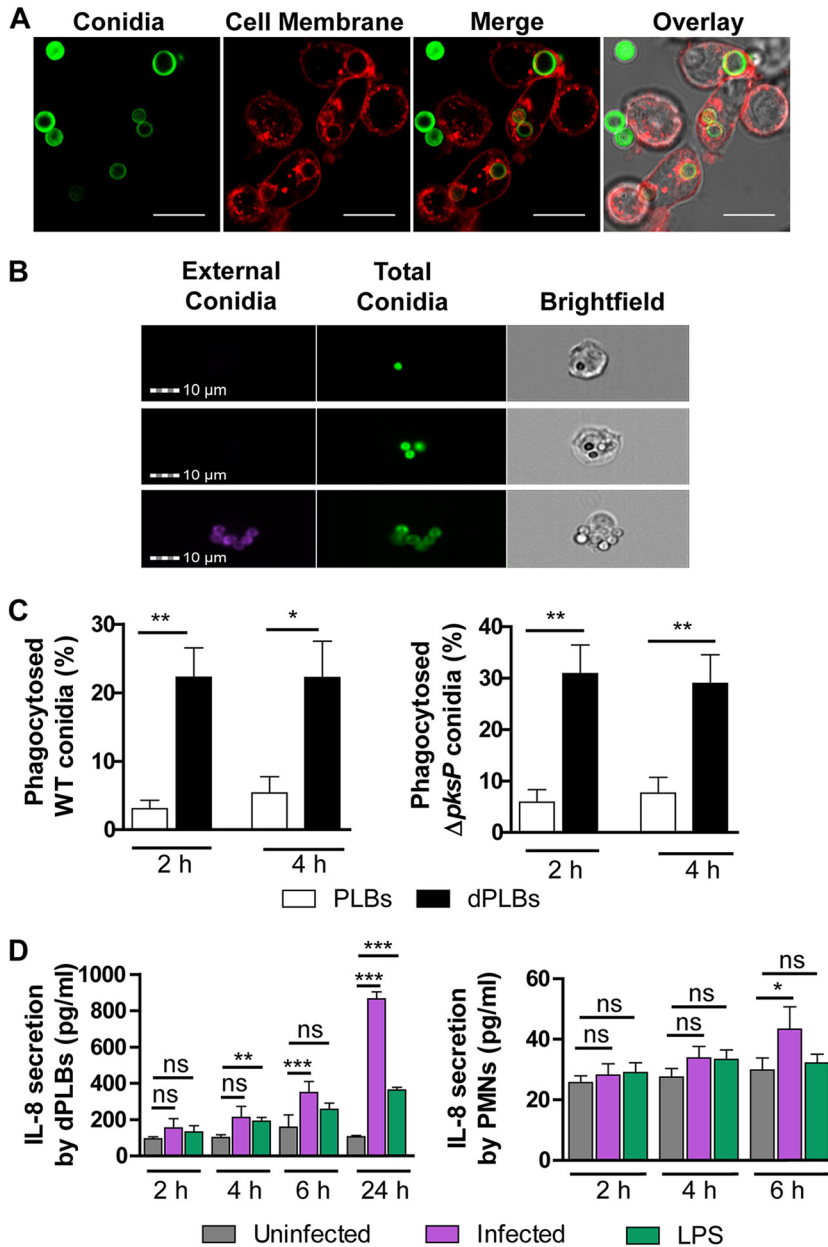
FIG 1 Phagocytosis of *A. fumigatus* conidia by PLB-985 cells. (A) Confocal microscopy images of wild-type conidia (FITC stained; green) phagocytosed by dPLB cells after 4 h coincubation. Membranes were stained with Cell Mask (red). Images are representative of three independent biological experiments. Bars, 10 μm. (B) Representative images of wild-type FITC-stained conidia phagocytosed by dPLB cells after 4 h coinfection obtained by imaging flow cytometry (top two rows). External conidia are visualized by counterstaining with CFW (purple), as seen in the bottom row. Images are representative of three independent experiments. (C) Quantification of PLB-985 cell phagocytosis using the IDEAS software on 5,000 cells per condition with either wild-type (WT) or Δ*pksP* conidia. Values are means plus standard errors of the means (SEM) (error bars) of four independent experiments. (D) ELISA detection of IL-8 cytokine released from infected dPLBs and primary human PMNs at different time points. Lipopolysaccharide (LPS) was included for comparison of a bacterial stimulus. Data are presented as means ± SEM from six biological replicates. Statistical significance is indicated as follows: *, $P \leq 0.05$; **, $P \leq 0.01$; ***, $P \leq 0.001$; ns, not significant.

results suggested that DMF-differentiated PLB-985 cells could serve as a suitable model for *A. fumigatus* pathogenesis and warranted further investigation.

Internalized *A. fumigatus* conidia are processed inside dPLB phagolysosomes.
Following internalization of conidia by professional phagocytes like macrophages and

neutrophils, conidia-containing phagosomes fuse with lysosomes to acidify the compartment and aid in fungal killing. Numerous additional enzymes are activated upon phagolysosomal acidification to degrade and digest the internalized fungal conidia. The acidification and maturation of phagolysosomes are regulated by protein complexes assembled on the phagolysosomal membrane, including lysosome-associated membrane protein 1 (LAMP-1), 2, and 3; several vacuolar ATPases (V-ATPases); Ras-related protein 5 (RAB5) and 7; flotillin 1 and 2; and numerous others (26). DHN-melanin on the surface of conidia can interfere with these processes in alveolar macrophages, monocytes, and primary neutrophils to delay fungal processing and phagolysosomal acidification (14). To test whether dPLB cells process conidia similarly to primary human PMNs, we first stained the cells with LAMP-1, a general endocytic marker on the membranes of phagolysosomes. LAMP-1 showed a clear signal around phagolysosomes of infected cells (Fig. 2A), and the intensity of the signal did not differ between wild-type and Δ*pksP* conidia (Fig. 2B). Furthermore, loading of dPLB cells with Lysotracker, a weak base that becomes fluorescent under acidic conditions, showed that the Δ*pksP* conidia-containing phagosomes were significantly more acidified than those containing wild-type conidia, revealing that DHN-melanin can also block the acidification process in the dPLB model as well (Fig. 2C to D).

The interference of the acidification pathway in alveolar macrophages by fungal DHN-melanin occurs through the inhibition of V-ATPase assembly (27, 28). This multiprotein complex plays a major role in lowering the pH from 6 to <4.5 by pumping H^+ ions across the phagolysosomal membrane. Staining of the V-ATPase V1 subunit in dPLB cells revealed that the percentage of recruitment to conidia-containing phagolysosomes was fairly similar for wild-type and Δ*pksP* conidia (Fig. S3A and S3B), suggesting that other proton pumps may contribute to acidification of these phagolysosomes in neutrophil-like cells. An additional defense mechanism for intraphagosomal degradation of pathogens occurs via reactive oxygen species (ROS) production. As expected, we observed dPLB cells to be capable of producing ROS after staining with CellROX Orange (Fig. S3C), consistent with the literature (29, 30).

***A. fumigatus* triggers formation of NETs from dPLB cells.** One defense mechanism employed by neutrophilic granulocytes to fight against pathogens is the formation of NETs. These structures consist of condensed chromatin and various enzymes that are released into the extracellular space and typically correlate with death of the cell (31). NETs contain several antifungal proteins, which are responsible for the fungistatic effect against *A. fumigatus* hyphae (16). To test whether dPLBs are also able to form NETs in response to *A. fumigatus* and serve as a model for this pathway, we coincubated dPLB cells with hyphae and stained for nucleic acid with 4′,6-diamidino-2-phenylindole (DAPI) (Fig. 3A). For a positive control, we induced NET formation using phorbol myristate acetate, a known trigger of NET formation in PLB-985 cells (Fig. 3B) (22, 32). We observed the presence of histone H3 embedded in the DNA fibers and an association of NETs with fungal hyphae (Fig. 3B). Taken together, these results showed that *A. fumigatus* is able to trigger NET formation in dPLB cells and that these NETs are specifically directed against the hyphae.

dPLB cells produce extracellular vesicles in response to infection. Recently, a new defense mechanism from neutrophilic granulocytes was discovered, the production of antimicrobial extracellular vesicles (33, 34). These small lipid-enclosed nanoparticles are released from primary PMNs after contact with microorganisms and, in the case of *A. fumigatus* conidia, can inhibit fungal growth after coincubation (10). This effect is likely due in part to their protein cargo, which consists of antimicrobial peptides such as myeloperoxidase, azurocidin, and cathepsin G. To assess whether dPLB cells can produce extracellular vesicles spontaneously or in response to *A. fumigatus*, we incubated cells with or without conidia for 2 and 4 h. Next, we isolated extracellular vesicles using two different methods; first using a previously described differential centrifugation-based approach (DC) (10) that enriches for medium-sized extracellular vesicles and a second approach that relies on size exclusion chromatography (SEC) to purify a more selective population of smaller extracellular vesicles. Using these methods, dPLB cells were observed to actively secrete extracellular
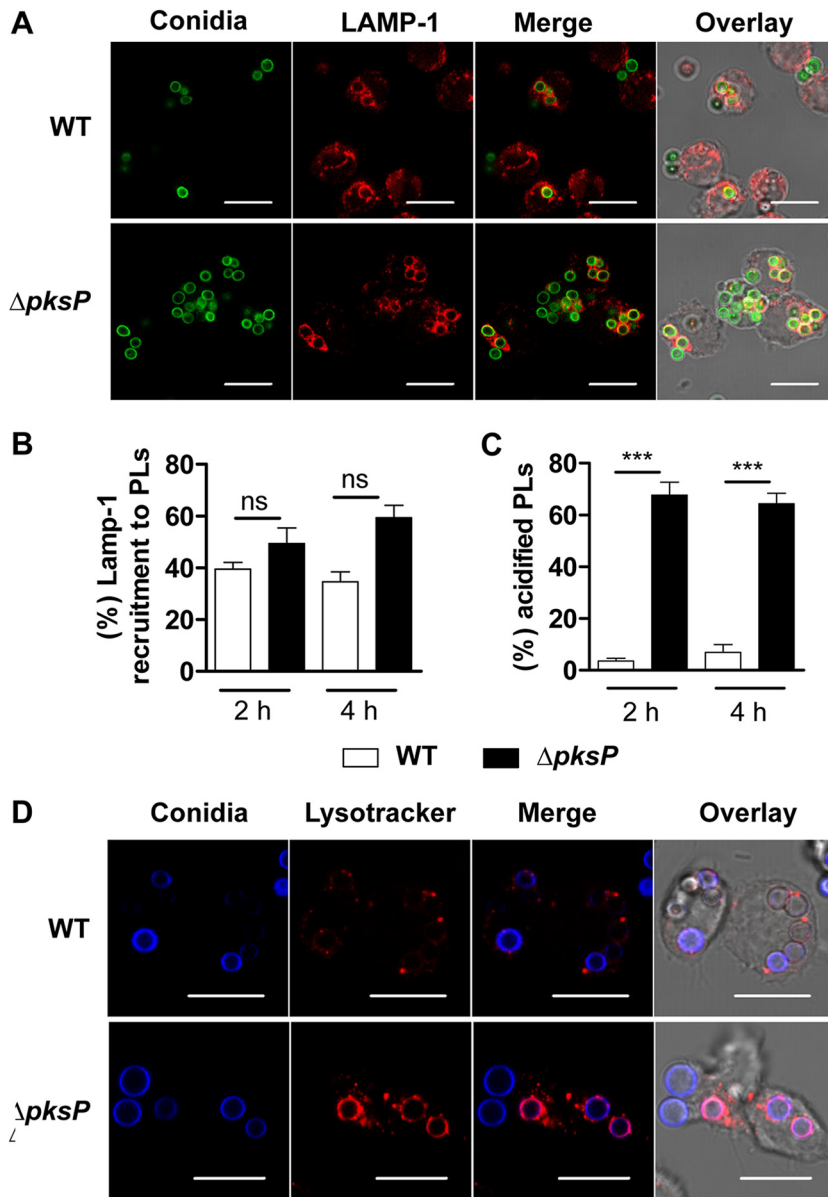
FIG 2 Processing of *A. fumigatus* conidia inside phagolysosomes. (A) dPLB cells were stained with LAMP-1 (red) after infection with wild-type (WT) or Δ*pksP* conidia (FITC labeled; green) for 4 h. Images are representative of three biological replicates. (B and C) Quantification of LAMP-1 colocalization with CFW-labeled conidia in phagolysosomes (B) and percentage of acidified conidia in dPLB cells after 2 and 4 h postinfection with wild-type and Δ*pksP* conidia (C). Data for panels B and C are presented as means plus SEM. Statistical significance is indicated as follows: *** = $P < 0.001$; ns, not significant. (D) Colocalization of conidia (CFW; blue) in acidified compartments labeled with Lysotracker (red). Images are representative of three biological replicates. Bars, 10 μm.

vesicles over time in a manner comparable to primary human PMNs (Fig. 4A and B). Using nanoparticle tracking analysis, we observed the median size of particles to be around 200 nm, similar to extracellular vesicles derived from primary neutrophils, a feature that was comparable between infection-derived and spontaneously released extracellular vesicles (Fig. 4C to D).

We next compared the protein content of dPLB-derived extracellular vesicles isolated at the 2-h time point using each isolation method with and without fungal infection by LC-MS/MS-based proteomics analysis. We were able to identify 1,984 unique proteins across all four samples (see Data Set S1 in the supplemental material). The majority of identified proteins (737 proteins) were found in all four samples (Fig. 5A). We
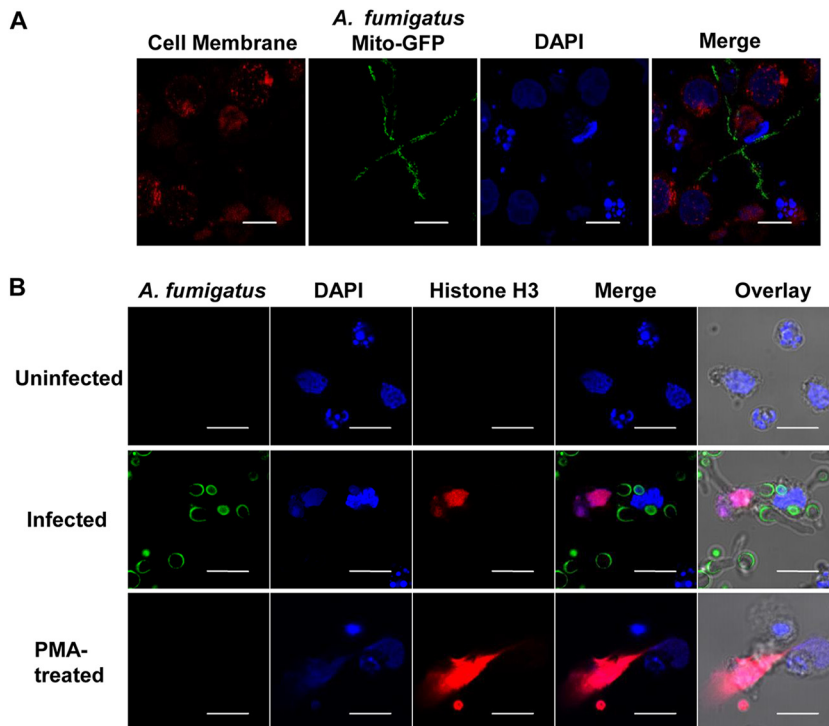
FIG 3 Production of NETs in response to *A. fumigatus* infection. (A) Confocal scanning laser microscopy of nucleic acid stained with DAPI (blue) released from dPLB cells stained with Cell Mask (red) after challenge with fungal hyphae containing a mitochondrial GFP reporter (*A. fumigatus* strain AfS35/pJW103 expressing a mitochondrial GFP reporter; green). Phorbol myristate acetate (PMA) was used as a positive control. Data are representative of three biological replicates. (B) Confocal micrographs of NET markers, histone H3 (red) and nucleic acid stained with DAPI (blue), produced by dPLB cells after contact with *A. fumigatus* hyphae (FITC labeled; green). Images are representative of three biological replicates. Bars, 10 μm.

expected that isolation using size exclusion chromatography would improve the quality of the isolated particles as has been shown previously (35), and this was in fact the case. We observed an increase in extracellular vesicle markers like the CD63 and CD81 tetraspanins and tumor susceptibility gene 101 (TSG101), and a decrease in cytoplasmic proteins like calnexin (CANX) (Table 1).

Extracellular vesicles produced by primary PMNs in response to *A. fumigatus* infection are known to be enriched for antimicrobial cargo proteins like azurocidin, cathepsin G, and defensin (10). In line with the primary neutrophil data, we found that dPLBs also contained many of the same proteins in both infection-derived and spontaneously released extracellular vesicles (Table 1), as evidenced by an UpSetR plot showing overlapping protein cohorts (Fig. S4) (10), albeit with some exceptions. For example, dPLBs appeared to lack defensin, neutrophil elastase, and some histone proteins previously observed. Ultimately, improvements in LC-MS/MS technology and the advantage of higher input amounts of extracellular vesicle protein using large amounts of dPLB cells in culture resulted in significantly more proteins detected here compared to efforts using primary neutrophils (10), proving that dPLBs offer a scalable system for the elucidation of novel mechanisms of neutrophil extracellular vesicle biology.

dPLB extracellular vesicles produced against *A. fumigatus* limit fungal growth. The most compelling feature of infection-derived extracellular vesicles of human neutrophils is likely their antifungal capacity, as we previously reported (10). We set out to determine whether the extracellular vesicles produced by dPLB cells in response to opsonized *A. fumigatus* conidia are antifungal to a mitochondrial-GFP (green fluorescent protein) reporter strain used previously as a marker of fungal
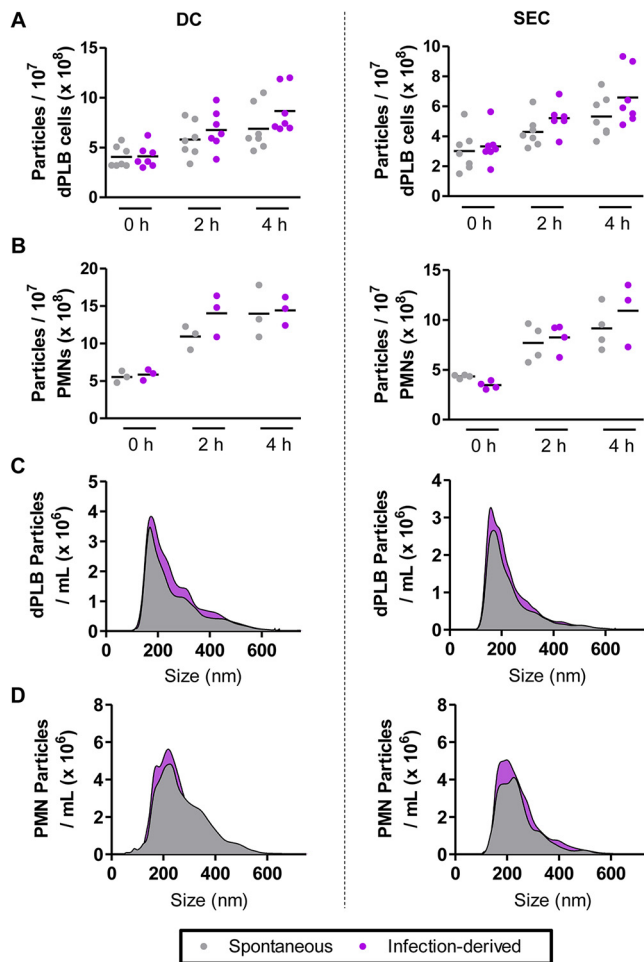
FIG 4 dPLB cells produce extracellular vesicles comparable in size to primary human PMNs. Extracellular vesicles released spontaneously or produced in response to infection with opsonized *A. fumigatus* conidia were isolated using a differential centrifugation-based approach (DC) or a size exclusion chromatography-based approach (SEC) and quantified using nanoparticle tracking analysis. (A and B) Extracellular vesicles were quantified from dPLB cells (A) or primary human PMNs (B) at 0, 2, and 4 h postinfection and show the mean of at least six biological replicates and three biological replicates, respectively. Each point indicates the value acquired in a single biological replicate. (C and D) Representative size histograms from five biological replicates are shown for extracellular vesicles derived from dPLB cells (C) and primary human PMNs (D).

viability (36). First, we incubated the reporter strain with dPLB cells and primary human PMNs and assessed the capacity of the cells to control infection. PMNs were capable of minimizing fungal outgrowth after 22 h, whereas dPLBs did not completely contain fungal growth (Fig. 6A). We then assessed the antifungal capacity of the dPLB extracellular vesicles. For this experiment, extracellular vesicles from equal numbers of dPLBs and primary human PMNs were isolated using differential centrifugation and found to be antifungal against the mitochondrial-GFP reporter strain. This was evidenced by fragmentation of fungal mitochondria after administration of extracellular vesicles to germinating conidia, which were allowed to germinate for 6 h prior to overnight incubation with extracellular vesicles, 3 mM H_2O_2 as a positive control, or left untreated as a negative control (Fig. 6B). Although the mitochondrial reporter clearly indicated fragmentation, the extracellular vesicles from dPLBs did appear to be in some cases less effective in limiting the length of hyphae than those from primary PMNs. It is important to note that dPLBs produced slightly fewer extracellular vesicles, which could partially explain the decreased antifungal activity in these assays (Fig. 6B). Additional representative images of dPLB-derived extracellular
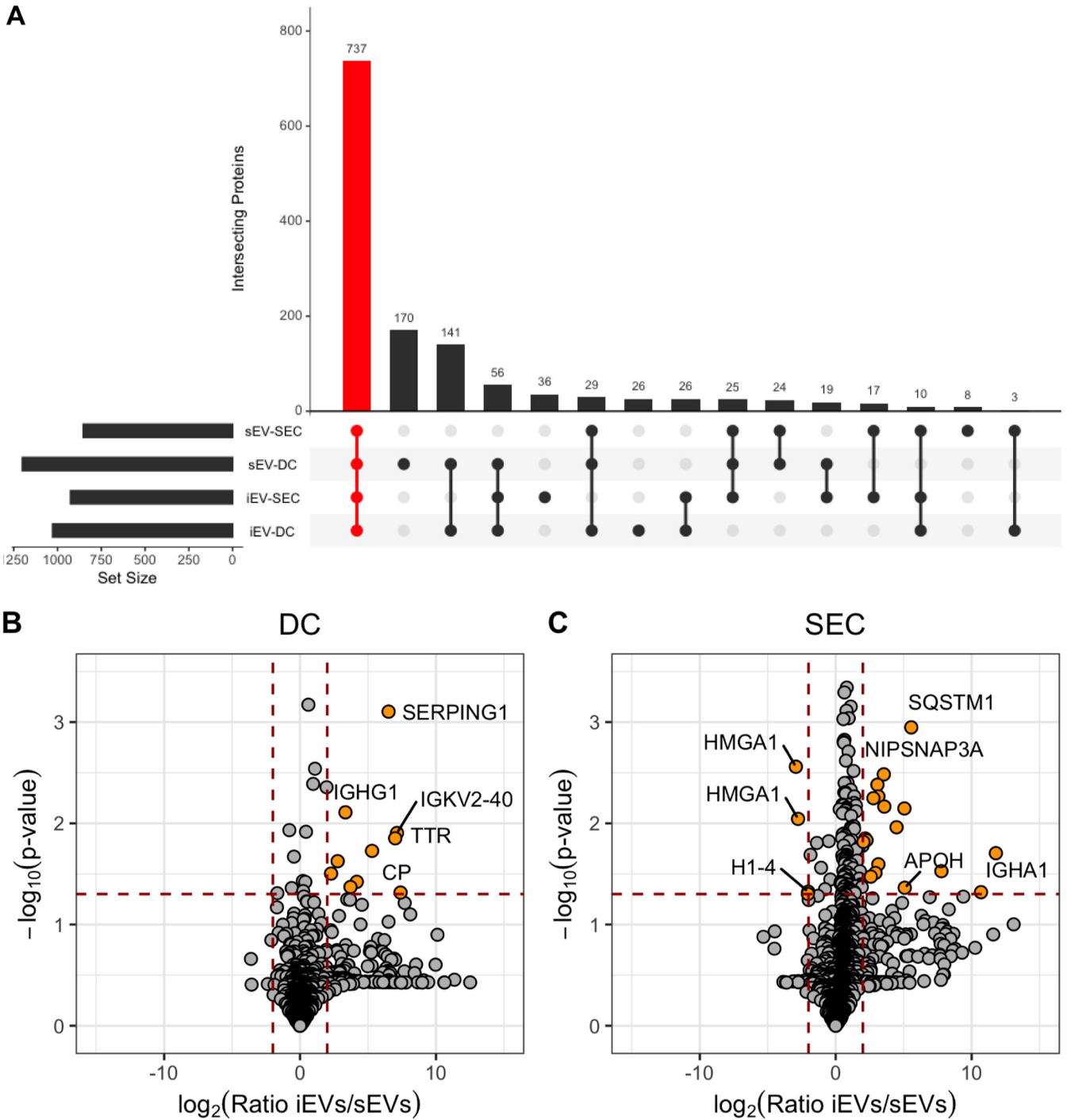
FIG 5 SEC enriches for extracellular vesicle populations. LC-MS/MS proteomics analysis was performed on extracellular vesicles isolated from dPLB cells using a differential centrifugation-based approach (DC) or a size exclusion chromatography-based approach (SEC) in the presence or absence of infection with opsonized *A. fumigatus* conidia. (A) Proteins identified in spontaneously released extracellular vesicles (sEVs) and infection-derived extracellular vesicles (iEVs) from at least two replicates of a given sample were intersected using UpSetR. The red bar indicates proteins that were found in all four samples. (B and C) Volcano plots show the $\log_2$ ratio of infection-derived extracellular vesicles (iEVs) versus spontaneously released EVs (sEVs) for DC-based isolation (B) and SEC-based isolation (C). Input data included values from all replicates using the RMN data included in Data Set S1 in the supplemental material. Plots were created using ggplot2 in R. Proteomics data are from three analytical replicates of three independent biological replicates. Orange circles represent proteins with greater than twofold change and *P* value of ≤0.05. Selected proteins are named for clarity.

vesicles are shown to indicate the spectrum of phenotypes observed for each experimental condition (Fig. S5). Collectively, these results suggest that dPLB infection-derived extracellular vesicles can limit *A. fumigatus* hyphal growth, similar to primary human PMNs (10).

TABLE 1 RMN fold change of selected proteins identified in extracellular vesicles from dPLB cells[a]

Marker type and gene	Accession no.	No. of infection-derived EVs (DC)/no. of spontaneous EVs (DC)	No. of infection-derived EVs (SEC)/no. of spontaneous EVs (SEC)	No. of infection-derived EVs (SEC)/no. of infection-derived EVs (DCs)	No. of spontaneous EVs (SEC)/no. of spontaneous EVs (DC)
EV markers					
CD63	F8VWK8	1.274	1.424	1.478	1.323
TSG101	F5H442	1.215	1.630	1.554	1.158
CD81	E9PRJ8	1.150	1.413	2.055	1.673
Non-EV markers					
CANX (calnexin)	P27824	−1.031	−1.082	−1.468	−1.398
MPO (myeloperoxidase)	P05164	−1.024	1.026	2.063	1.963
CTSG (cathepsin G)	P08311	1.045	1.042	1.117	1.120
AZU1 (azurocidin)	P20160	−1.141	1.029	1.521	1.295

[a]Abbreviations: EVs, extracellular vesicles; DC, differential centrifugation-based approach; SEC, size exclusion chromatography-based approach.

DISCUSSION

Neutrophils are critical players in the immune response to fungal pathogens stemming from their numerous antimicrobial capacities (10, 37). To study neutrophil functions, numerous cell lines that model these abilities *in vitro* have been considered with limited success. The most promising are the HL-60 leukemia cell line and PLB-985 sublineage, which have been used as models for aspergillosis and bacterial killing (22–24, 29). In this study, we analyzed different aspects of the interaction between DMF-differentiated PLB-985 myeloid cells and the fungus *A. fumigatus* for the first time, making frequent comparisons with data from primary neutrophils.

Primary neutrophils are capable of phagocytosing and processing *A. fumigatus* conidia, features that were maintained in dPLB cells. As expected for cultured cells, the observed phagocytosis rate of *A. fumigatus* conidia by dPLB cells was lower than that of primary human PMNs. It is possible that additional differentiation methods will ultimately reveal higher rates of phagocytosis, as PLB-985 cells differentiated with DMF are known to exhibit lower phagocytic activity than cells differentiated with dimethyl sulfoxide (38). In terms of cytokine release, we observed increased release of IL-8 from dPLBs after infection with opsonized *A. fumigatus* conidia, but not IL-1β, consistent with our observations of human PMNs. These results are also in agreement with those collected from primary PMNs coincubated with L-ficolin-opsonized conidia for 8 h, where secretion of IL-8 was also much higher than secretion of IL-1β (39).

We next stained dPLB cells for the endosomal marker LAMP-1 and measured the acidification of the phagolysosomes via Lysotracker to assess intracellular processing of fungal conidia. These experiments confirmed that around 20% of wild-type conidia are completely internalized inside the phagosomes and that lysosomal fusion occurs as a next step of conidial processing. Interestingly, and as already demonstrated for primary monocytes and neutrophils (14), melanized conidia showed less acidification around the phagolysosomal membrane than the mutant lacking DHN-melanin. This effect in monocytes is caused by inhibition of V-ATPase assembly. Surprisingly, staining for the V1 subunit of the V-ATPase did not reveal a significant difference between the wild-type and $\Delta pksP$ strains in dPLB cells as has been observed in other cell systems. These results suggest that neutrophils potentially employ additional mechanisms to acidify phagolysosomes in neutrophilic granulocytes after *A. fumigatus* infection or that the methods used were not sufficiently sensitive to detect slight differences in acidification. Together, these results suggest that dPLBs can serve as an intriguing model to study various aspects of neutrophil phagocytosis and intracellular processing in a more tractable *in vitro* model system.

A conidium that escapes phagocytosis can sometimes germinate into a hypha, a morphotype that is much more difficult to eliminate and requires the antifungal activity of neutrophils. One mechanism that aids in control of *A. fumigatus* hyphae is the release of fungistatic NETs composed of DNA and antimicrobial proteins. By staining for extracellular DNA and NET constituent histone H3, we could clearly show that dPLB cells also produce NETs in response to *A. fumigatus* hyphae, comparable to primary
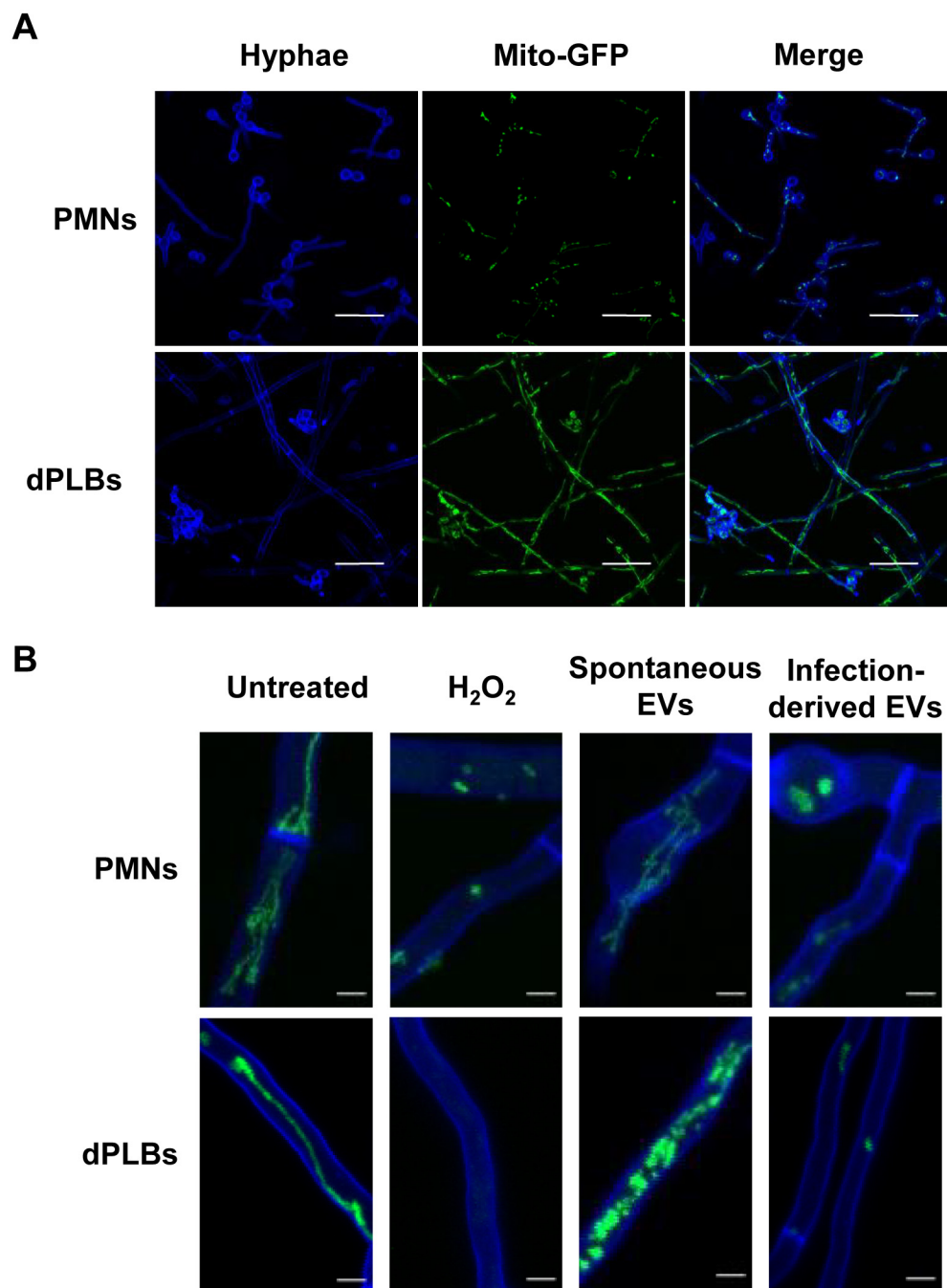
A

B

FIG 6 Infection-derived extracellular vesicles from dPLBs are antifungal to *A. fumigatus* hyphae. (A) Conidia from *A. fumigatus* strain AfS35 containing plasmid pJW103 expressing a mitochondrial GFP reporter (green) were opsonized and coincubated with freshly harvested human PMNs or dPLBs. After overnight incubation (22 h), samples were stained with CFW for 10 min, and images were taken using a Zeiss LSM 780 confocal microscope. Bars, 20 μm. (B) The *A. fumigatus* strain AfS35 expressing a mitochondrial GFP reporter (green) was first grown for 6 h and then incubated overnight with spontaneously released extracellular vesicles or infection-derived extracellular vesicles isolated from primary human PMNs or dPLBs. Fungal hyphae were then stained with CFW. For a control, untreated hyphae and hyphae treated with 3 mM H_2O_2 to induce cell death are included. An intact mitochondrial network is shown by a filamentous network, whereas a disrupted network is shown by fragmentation or the lack of green signal. Bars, 5 μm.

human PMNs and in agreement with other studies challenging dPLBs with bacterial pathogens (22, 23).

Production of extracellular vesicles from primary neutrophils coincubated with *Aspergillus* conidia or bacteria like *Staphylococcus aureus* is an important defense

strategy against microorganisms (10, 33). We found that dPLB cells were also able to generate comparable populations of extracellular vesicles to PMNs upon contact with opsonized conidia. Accumulation of extracellular vesicles of approximately 200 nm in diameter was observed over time, independently of the isolation method we applied. Proteomics analysis revealed that by using a size exclusion chromatography-based isolation approach, the extracellular vesicle population could be enriched for extracellular vesicle marker proteins like CD63, CD81, and TSG101. We observed that the samples obtained by this method had a higher abundance of proteins and showed more differences between the spontaneously released and infection-derived extracellular vesicles. In particular, infection-derived extracellular vesicles were enriched in immunoglobulins and complement factors compared to spontaneously released vesicles. These serum proteins may be introduced to the infection system during opsonization of the fungal conidia despite thorough washing. It remains unclear whether these immunoglobulins and complement factors play an important role in extracellular vesicle biology during *A. fumigatus* infection. As a hint for such a role, the association of immunoglobulins and complement proteins was shown previously to be important in systemic lupus erythematosus (SLE) disease, where extracellular vesicles with immunoglobulin cargo acted as immune complexes to mediate inflammation (40, 41).

In the proteomics analysis of extracellular vesicles derived from primary neutrophils infected with *A. fumigatus*, several antimicrobial peptides, such as cathepsin G and azurocidin, were detected (10). Coincubation of these extracellular vesicles from primary neutrophils with fungal hyphae arrested growth, which we confirmed here. Using dPLB cells, we identified extracellular vesicles containing cathepsin G and azurocidin; however, the distribution remained relatively equal between spontaneously released and infection-derived extracellular vesicles. We suspect that this is due to the differentiation procedure of dPLB cells with DMF, which provides a mild inflammatory stimulus. Nevertheless, we observed mitochondrial damage in hyphae treated with infection-derived but not spontaneously released extracellular vesicles. We can postulate several reasons for this result. First, it is possible that immunoglobulins are playing a role in targeting extracellular vesicles to fungal hyphae. In this case, the protein cargo may be the same, but targeting would be inefficient in spontaneously released extracellular vesicles. Of note, opsonization of the bacterial pathogen *Staphylococcus aureus* was not found to influence the antimicrobial capacity of neutrophil-derived extracellular vesicles (33). A second option is that additional extracellular vesicle cargo molecules such as RNA or lipids may play a role in the antifungal activity. It has been shown in many instances that extracellular vesicles can contain small RNAs that exert distinct functions during infection, especially in regard to plant fungal pathogens (42, 43). We believe that a combination of factors is likely involved in the antifungal effect of extracellular vesicles.

Part of the explanation may also come from similarities between neutrophilic granules and extracellular vesicles. Granules and extracellular vesicles are distinct cellular features, but they do share some biogenesis pathways and cargo molecules. For example, the azurophilic granules contain myeloperoxidase to aid in pathogen killing in the endocytic pathway via fusion of the granules to pathogen-containing phagosomes (44), but myeloperoxidase is also released in a CD63-negative population of extracellular vesicles known as microvesicles (45). Based on the proteomics analysis of this study, as well as our previous work (10), it seems possible that microvesicle cargo proteins like myeloperoxidase contribute at least in part to the antifungal activity. However, the presence of myeloperoxidase in spontaneously released extracellular vesicles and the lack of susceptibility of patients lacking myeloperoxidase to fungal infections (46) hint that other factors are also involved. Besides, the shared marker protein CD63 nicely highlights another link between granules and extracellular vesicles, the shared biogenesis from multivesicular bodies of azurophilic granules and the extracellular vesicle subset called exosomes (47).

In conclusion, our results suggest that DMF-differentiated PLB-985 cells can be used as a model to study aspects of the interaction of the human-pathogenic fungus

A. fumigatus with neutrophilic granulocytes. Although they will never substitute for all experiments with neutrophils, we do believe that this system will serve as a useful tool for the genetic dissection of *A. fumigatus* pathogenesis in the future.

MATERIALS AND METHODS

Fungal strain cultivation and opsonization. Cultivation of *A. fumigatus* strains CEA10 (Fungal Genetics Stock Center; A1163), CEA17 Δ*akuB^{ku80}* Δ*pksP* (48), and AfS35/pJW103 (36) was performed on malt agar plates (Sigma-Aldrich) supplemented to a final concentration of 2% (wt/vol) agar for 5 days at 37°C. Conidia were harvested in sterile, ultrafiltrated water filtered through a 30-μm pore filter (MACS, Miltenyi Biotec). Prior to confrontation with PLB-985 cells, conidia were opsonized with normal human serum (Merck Millipore). Briefly, 900 μl of spore suspension was mixed with 100 μl of normal human serum and incubated in a thermomixer at 37°C for 30 min shaking at 500 rpm. The spore suspension was washed three times by collecting spores via centrifugation at 1,800 $\times$ *g* for 1 min at 4°C and resuspending in fresh phosphate-buffered saline (PBS). Following washing, spores were enumerated in a Thoma chamber in preparation for infection assays.

Cell culture cultivation, differentiation, and infection. PLB-985 cells were maintained in Roswell Park Memorial Institute medium 1640 (RPMI; Gibco) supplemented with 10% (vol/vol) fetal bovine serum (FBS; HyClone, GE Life Science), 100 U/ml penicillin-streptomycin antibiotic solution (Lonza), and 2 mM UltraGlutamine (alanyl L-glutamine; Gibco). For differentiation into a neutrophilic granulocyte cell type, 4×10^5 cells/ml were resuspended in supplemented RPMI containing 2.5% (vol/vol) FBS and 0.5% DMF (Sigma-Aldrich) for 4 days at 37°C with 5% (vol/vol) CO_2. On day 4, fresh differentiation medium was added, and the cells were incubated for 3 additional days. On day 7, cells were collected, centrifuged at 300 $\times$ *g* for 5 min, and then seeded in wells for experiments at the appropriate concentrations. The medium used for all the assays was composed of RPMI supplemented with 1% (vol/vol) exosome-depleted FBS (Life Technologies GmbH), 2 mM UltraGlutamine, and 0.5% (vol/vol) DMF.

Isolation of human PMNs. Fresh venous blood was drawn from adult healthy volunteers, aged 20 to 35 years, after obtaining written consent. This study was approved by the Jena University Hospital Institutional Review Board (approval number 5074-02/17) in agreement with the Declaration of Helsinki. Blood was collected in EDTA BD Vacutainer tubes (BD Biosciences) and mixed with PBS. Six milliliters of this solution was carefully layered onto (avoiding any mixing) 5 ml (1:1 [vol/vol]) of PolymorphPrep solution (Progen) and centrifuged 50 min at 500 $\times$ *g* for gradient separation. After centrifugation, the neutrophil layer was collected, mixed with an equal volume of 0.5% PBS, and recentrifuged for 15 min at 400 $\times$ *g*. To limit contamination of red blood cells, the pellet was lysed with the ACK lysis buffer (Gibco) and centrifuged as before. The PMNs were finally resuspended in RPMI medium without phenol red (Thermo Fisher Scientific) and after addition of trypan blue counted with a Luna automated cell counter (Logos Biosystem). For each experiment, the viability of neutrophils was ≥95%.

Phagocytosis assays. To assess phagocytic ability, we used a combination of imaging flow cytometry and confocal fluorescence microscopy. For both methods, the conidia were first stained with fluorescein isothiocyanate (FITC) and then after confrontation of dPLBs or primary neutrophils, counterstained with calcofluor white (CFW; Sigma-Aldrich). The FITC solution was obtained by dissolving FITC powder (Sigma-Aldrich) in 5 ml of 0.1 M sodium carbonate (Na_2CO_3), followed by filtration through a 0.22-μm-pore-size filter (Carl Roth). Afterwards 1 ml of this solution was mixed with 500 μl of spore suspension and incubated for 30 min at 37°C while shaking at 1,000 rpm in the dark. The spores were then pelleted and washed three times with PBS with 0.001% (vol/vol) Tween 20 (Carl Roth). During the last washing step, Tween was removed to avoid residual detergent in the samples (14, 49). Before counting, the conidia were opsonized following the protocol described above. Spores were then added to cells and coincubated for 2 and 4 h at 37°C with 5% (vol/vol) CO_2. At each time point, CFW was added to a final concentration of 1 μg/ml and incubated for 1 min. Afterwards the cell suspension was transferred to microcentrifuge tubes, centrifuged at 600 $\times$ *g* for 2 min at 4°C, and washed with PBS twice. After the supernatant was discarded, the pellet was fixed with 150 μl of 3.7% (vol/vol) formaldehyde in PBS at room temperature for 15 min and subsequently washed as described above. For imaging flow cytometry measurements, the cells were resuspended in 150 μl of PBS and analyzed immediately or stored at 4°C for no more than 24 h. Four independent experiments were performed, and for each replicate, 5,000 cells were analyzed using the ImageStream X Mark II (Luminex). A 488-nm laser was used to detect FITC staining, and a 405-nm laser was used to detect CFW staining. The laser voltage was adjusted depending on the sample. For wild-type conidia, we used 10 mW of 488-nm laser and 2 mW for the 405-nm laser, and for Δ*pksP* conidia, we used 1 and 2 mW of the respective lasers. The fluorescence intensities of the samples were compensated and analyzed with the IDEAS software (Luminex). An example of the gating strategy used for analysis is provided (see Fig. S1B and S1C in the supplemental material). For the fluorescence microscopy analysis, cells were seeded in 8-well μ-slides (Ibidi) and visualized using a Zeiss LSM 780 confocal microscope (Carl Zeiss) from at least three biological replicates.

Immunofluorescence assays. For immunofluorescence assays, cells were allowed to adhere in a 24-well plate with poly-L-lysine-coated glass coverslips for 1 h (Merck). After infection with labeled *A. fumigatus* spores and incubation for the noted times, cells were fixed using 3.7% (vol/vol) formaldehyde in PBS for 10 min, rinsed three times with PBS, permeabilized for 15 min using 0.1% (vol/vol) Triton X-100 in PBS or 0.1% (wt/vol) saponin in PBS, and then blocked for 30 min with 2% (wt/vol) bovine serum albumin (BSA). After permeabilization, washed cells were incubated with primary rabbit anti-Lamp-1 antibody (Abcam ab24170; 1:100 dilution), anti-V-ATPase V1 subunit antibody (Abcam ab73404; 1:100 dilution), or anti-histone H3 (Cell Signaling DIH2; 1:200 dilution) antibody in 1% (wt/vol) BSA in PBS,

followed by incubation with secondary goat anti-rabbit IgG antibody DyLight 633 (Thermo Fisher Scientific). The glass coverslips were mounted onto microscopy slides and visualized using a Zeiss LSM 780 confocal microscope (Carl Zeiss). LAMP-1 recruitment was quantified by comparing the positive signal from stained phagolysosomes to nonstained phagolysosomes.

Reactive oxygen species measurements. ROS production was detected in dPLB cells by seeding cells in 8-well μ-slides (Ibidi) coated with poly-L-lysine followed by infection with *A. fumigatus* conidia at a multiplicity of infection (MOI) of 5 for either 2 or 4 h. CellROX Orange Reagent (Thermo Fisher Scientific) was added 30 min prior to the end of the infection time points, and ROS production was imaged using a Zeiss LSM 780 confocal microscope (Carl Zeiss) for fluorescent intensity.

Cytokine measurement. For the detection of IL-8 and IL-1β, 2×10^5 dPLB cells or primary neutrophils were seeded in 24-well plates. After the addition of conidia at an MOI of 5, plates were incubated at 37°C with 5% (vol/vol) CO$_2$ for 2, 4, or 6 h. An additional 24-h time point was included for dPLB cells. For a positive control, cells were treated with 5 μg/ml of lipopolysaccharide (LPS; Sigma-Aldrich L4516). At the appropriate endpoint, samples were collected, centrifuged at $300 \times g$ for 5 min to remove cell debris, frozen at -20°C, and analyzed within 3 days. Cytokines were measured using human ELISA Max deluxe kits (BioLegend) according to the manufacturer's instruction.

Acidification assays. Acidification assays were performed as mentioned previously (28). Briefly, the cells were incubated with 50 nM Lysotracker DND-99 (Thermo Fisher Scientific) for 1 h prior to infection. After that, FITC-labeled conidia were added to the cells for 2 or 4 h and imaged using Zeiss LSM 780 confocal microscope (Carl Zeiss). For quantification, 200 conidia-containing phagolysosomes were counted and evaluated for acidification. The values represent the means $\pm$ standard errors of the means (SEM) of three separate experiments.

Extracellular vesicle isolation. After infection with *A. fumigatus*, the supernatant of dPLB cells was collected, and extracellular vesicles were isolated using two different methods: a differential centrifugation-based approach or a size exclusion chromatography-based approach. The first method was described previously for the isolation of neutrophil-derived extracellular vesicles (10, 33). In both approaches, samples were centrifuged at $3,000 \times g$ for 15 min at 4°C and filtered through 5-μm-pore-size filters (Carl Roth). In the first method, samples were then centrifuged at $19,500 \times g$ for 20 min at 4°C to collect extracellular vesicles. For the second approach, the clarified filtrate was concentrated using Amicon Ultra-15 centrifugal filters (Merck) with a molecular mass cutoff (MWCO) of 100 kDa for 10 min at 4°C and $3,220 \times g$ and loaded on size exclusion chromatography qEV 70-nm columns (Izon). After the 3-ml void volume was discarded, 1.5 ml of extracellular vesicle sample was collected and measured. When necessary, extracellular vesicles were further concentrated using 10-kDa cutoff Amicon Ultra 0.5-ml filters (Merck). Extracellular vesicles were used fresh for most of the downstream experiments except for proteomics analysis where they were frozen at -20°C.

Nanoparticle tracking analysis. Particle concentration and size distribution were analyzed using a nanoparticle tracking analysis (NTA) NS300 device with a 650-nm laser (Malvern Instruments Ltd.). Fresh samples were measured with a constant flow rate of 20 and a temperature set at 25°C. Five 60-s videos were recorded with a camera level of 11. Videos were then analyzed with the NTA 3.2.16 software using a detection threshold of 4.

Protein preparation for LC-MS/MS. Isolated extracellular vesicles were delipidated as described previously (10) using the protein precipitation protocol of Wessel and Flügge (50). Delipidated extracellular vesicles were resolubilized in 100 μl of 50 mM triethyl ammonium bicarbonate (TEAB) in 1:1 (vol/vol) trifluoroethanol-water. For reduction of cysteine thiols, the solution was mixed with 10 mM Tris(2-carboxyethyl) phosphine and alkylated with 12.5 mM chloroacetamide at 70°C for 30 min in the dark. Proteins were digested for 18 h at 37°C with trypsin-LysC mix (Promega) at a protein-to-protease ratio of 25:1. Tryptic peptides were first completely evaporated using a vacuum concentrator (Eppendorf) and then resolubilized in 0.05% (vol/vol) trifluoroacetic acid (TFA) in 2:98 (vol/vol) acetonitrile-water. Finally, the samples were filtered through Ultrafree-MC hydrophilic polytetrafluoroethylene (PTFE) membrane (0.2-μm pore size) spin filters (Millipore) and stored at -20°C until measurement. Each sample was measured in triplicate (three analytical replicates of three biological replicates) as follows.

LC-MS/MS analysis. LC-MS/MS analysis was performed on an Ultimate 3000 nano RSLC system connected to a QExactive HF mass spectrometer (both Thermo Fisher Scientific). Peptide trapping for 5 min on an Acclaim Pep Map 100 column (2 cm $\times$ 75 μm, 3 μm) at 5 μl/min was followed by separation on an analytical Acclaim Pep Map RSLC nano column (50 cm $\times$ 75 μm, 2 μm). Mobile phase gradient elution of eluent A (0.1% [vol/vol] formic acid in water) mixed with eluent B (0.1% [vol/vol] formic acid in 90/10 acetonitrile/water) was performed as follows: 0 min at 4% eluent B, 30 min at 12% eluent B, 75 min at 30% eluent B, 85 min at 50% eluent B, 90 to 95 min at 96% eluent B, and 95.1 to 120 min at 4% eluent B.

Positively charged ions were generated at spray voltage of 2.2 kV using a stainless-steel emitter attached to the Nanospray Flex Ion Source (Thermo Fisher Scientific). The quadrupole/orbitrap instrument was operated in full MS/data-dependent MS2 (Top15) mode. Precursor ions were monitored at m/z 300 to 1,500 at a resolution of 120,000 FWHM (full width at half maximum) using a maximum injection time (ITmax) of 120 ms and an AGC (automatic gain control) target of 3×10^6. Precursor ions with a charge state of $z = 2$ to 5 were filtered at an isolation width of m/z 1.6 atomic mass units (amu) for further higher-energy collisional dissociation (HCD) fragmentation at 27% normalized collision energy (NCE). MS2 ions were scanned at 15,000 FWHM (ITmax = 100 ms; AGC = 2×10^5). Dynamic exclusion of precursor ions was set to 25 s, and the underfill ratio was set to 1.0%. The LC-MS/MS instrument was controlled by Chromeleon 7.2, QExactive HF Tune 2.8, and Xcalibur 4.0 software.

Database search and data analysis. Tandem mass spectra were searched against the UniProt database of *Homo sapiens* (https://www.uniprot.org/proteomes/UP000005640; 17 May 2021) and *Neosartorya fumigata* (https://www.uniprot.org/proteomes/UP000002530; 17 May 2021) using Proteome Discoverer (PD) 2.4 (Thermo) and the algorithms of Mascot 2.4.1 (Matrix Science), Sequest HT (version of PD2.2), MS Amanda 2.0, and MS Fragger 3.2. Two missed cleavages were allowed for tryptic digestion. The precursor mass tolerance was set at 10 ppm, and the fragment mass tolerance was set at 0.02 Da. Modifications were defined as dynamic Met oxidation and protein N-terminal acetylation with and without methionine loss as well as static Cys carbamidomethylation. A strict false discovery rate (FDR) of $<$1% (peptide and protein level) were required for positive protein hits. If only one peptide per protein has been identified, the hit was accepted if the Mascot score was $>$30 or the MS Amanda score was $>$300 or the Sequest score was $>$4 or the MS Fragger score was $>$8. The Percolator node of PD2.4 and a reverse decoy database was used for q value validation of spectral matches. Only rank 1 proteins and peptides of the top scored proteins were counted. Label-free protein quantification was based on the Minora algorithm of PD2.2 using a signal-to-noise ratio of $>$5. Imputation of missing quantification values was applied by setting the abundance to 75% of the lowest abundance identified for each sample. Normalization was based on a replicate median total peptide sum approach, which was calculated based on the sum of all identified peptide abundance values per replicate sample. The sums of each of the three replicates from the four sample groups were used to calculate median values. Normalization factors were calculated by dividing median values of the respective sample group by the abundance sum of each sample. Normalization factors were multiplied with single protein abundance values of each replicate/sample. The P values are based on a Student`s t test. Ratio-adjusted P values were calculated by dividing P values with the $\log_4$ ratio of the protein abundance levels. Significant differences in protein abundance were defined when the following three requirements were reached: at least a fourfold change in abundance (up and down), a ratio-adjusted P value of $<$0.05, and identified in at least two of three replicates of the sample group with the highest abundance. Intersection plots were created using the UpSetR package (51) and include only proteins that were detected in at least two replicates of a given sample. Volcano plots were created using ggplot2 in R using the replicate median total peptide sum normalized (RMN) data for all proteins detected in Data Set S1 in the supplemental material.

Fungal mitochondrial reporter inhibition assay. To characterize growth inhibition and killing of hyphae by fungus-induced extracellular vesicles, an *A. fumigatus* strain expressing a mitochondrial GFP reporter (AfS35/pJW103 [36]) has been used as described previously (10). Extracellular vesicles produced by 1×10^7 dPLB cells or PMNs were isolated and coincubated with the reporter strain. After 16 h of incubation, samples were stained with CFW, and images were taken using Zeiss LSM 780 confocal microscope (Carl Zeiss).

Statistical analysis. Data were plotted and statistically analyzed using GraphPad Prism software 5.0 (GraphPad Software) unless otherwise noted. The Student's t test was used for significance testing when comparing two groups. Differences between the groups were considered significant at a P value of $<$0.05. Throughout the article, significance is denoted as follows: *, $P \leq 0.05$; **, $P \leq 0.01$; ***, $P \leq 0.001$; ns, not significant.

Ethics statement. Peripheral human blood was collected from healthy volunteers only after written informed consent was provided. The study was conducted in accordance with the Declaration of Helsinki and approved by the Ethics Committee of the University Hospital Jena (approval number 5074-02/17).

Data availability. The mass spectrometry proteomics data have been deposited to the ProteomeXchange Consortium via the PRIDE partner repository (52) with the data set identifier PXD027032.

SUPPLEMENTAL MATERIAL

Supplemental material is available online only.

DATA SET S1, XLSX file, 18.9 MB.
FIG S1, TIF file, 2.6 MB.
FIG S2, TIF file, 0.7 MB.
FIG S3, PDF file, 0.2 MB.
FIG S4, TIF file, 1 MB.
FIG S5, TIF file, 2 MB.
TABLE S1, DOCX file, 0.01 MB.

ACKNOWLEDGMENTS

REFERENCES

1. Brown GD, Denning DW, Gow NA, Levitz SM, Netea MG, White TC. 2012. Hidden killers: human fungal infections. Sci Transl Med 4:165rv13. https://doi.org/10.1126/scitranslmed.3004404.

2. Schmiedel Y, Zimmerli S. 2016. Common invasive fungal diseases: an overview of invasive candidiasis, aspergillosis, cryptococcosis, and Pneumocystis pneumonia. Swiss Med Wkly 146:w14281. https://doi.org/10.4414/smw.2016.14281.

3. Latge JP, Chamilos G. 2019. Aspergillus fumigatus and aspergillosis in 2019. Clin Microbiol Rev 33:e00140-18. https://doi.org/10.1128/CMR.00140-18.

4. Nasir N, Farooqi J, Mahmood SF, Jabeen K. 2020. COVID-19-associated pulmonary aspergillosis (CAPA) in patients admitted with severe COVID-19 pneumonia: an observational study from Pakistan. Mycoses 63:766–770. https://doi.org/10.1111/myc.13135.

5. Salmanton-Garcia J, Sprute R, Stemler J, Bartoletti M, Dupont D, Valerio M, Garcia-Vidal C, Falces-Romero I, Machado M, de la Villa S, Schroeder M, Hoyo I, Hanses F, Ferreira-Paim K, Giacobbe DR, Meis JF, Gangneux JP, Rodriguez-Guardado A, Antinori S, Sal E, Malaj X, Seidel D, Cornely OA, Koehler P, FungiScope European Confederation of Medical Mycology/The International Society for Human and Animal Mycology Working Group. 2021. COVID-19-associated pulmonary aspergillosis, March-August 2020. Emerg Infect Dis 27:1077–1086. https://doi.org/10.3201/eid2704.204895.

6. Rivera A, Hohl TM, Collins N, Leiner I, Gallegos A, Saijo S, Coward JW, Iwakura Y, Pamer EG. 2011. Dectin-1 diversifies Aspergillus fumigatus-specific T cell responses by inhibiting T helper type 1 CD4 T cell differentiation. J Exp Med 208:369–381. https://doi.org/10.1084/jem.20100906.

7. Brakhage AA, Langfelder K. 2002. Menacing mold: the molecular biology of Aspergillus fumigatus. Annu Rev Microbiol 56:433–455. https://doi.org/10.1146/annurev.micro.56.012302.160625.

8. Drummond RA, Gaffen SL, Hise AG, Brown GD. 2014. Innate defense against fungal pathogens. Cold Spring Harb Perspect Med 5:a019620. https://doi.org/10.1101/cshperspect.a019620.

9. Mircescu MM, Lipuma L, van Rooijen N, Pamer EG, Hohl TM. 2009. Essential role for neutrophils but not alveolar macrophages at early time points following Aspergillus fumigatus infection. J Infect Dis 200:647–656. https://doi.org/10.1086/600380.

10. Shopova IA, Belyaev I, Dasari P, Jahreis S, Stroe MC, Cseresnyes Z, Zimmermann AK, Medyukhina A, Svensson CM, Kruger T, Szeifert V, Nietzsche S, Conrad T, Blango MG, Kniemeyer O, von Lilienfeld-Toal M, Zipfel PF, Ligeti E, Figge MT, Brakhage AA. 2020. Human neutrophils produce antifungal extracellular vesicles against Aspergillus fumigatus. mBio 11:e00596-20. https://doi.org/10.1128/mBio.00596-20.

11. McCormick A, Heesemann L, Wagener J, Marcos V, Hartl D, Loeffler J, Heesemann J, Ebel F. 2010. NETs formed by human neutrophils inhibit growth of the pathogenic mold Aspergillus fumigatus. Microbes Infect 12:928–936. https://doi.org/10.1016/j.micinf.2010.06.009.

12. Brogan TD. 1964. Effect of complement and of the carbohydrate components of sputum on phagocytosis by human polymorphonuclear leucocytes. Immunology 7:626–638.

13. Pazhakh V, Ellett F, Croker BA, O'Donnell JA, Pase L, Schulze KE, Greulich RS, Gupta A, Reyes-Aldasoro CC, Andrianopoulos A, Lieschke GJ. 2019. Beta-glucan-dependent shuttling of conidia from neutrophils to macrophages occurs during fungal infection establishment. PLoS Biol 17:e3000113. https://doi.org/10.1371/journal.pbio.3000113.

14. Thywißen A, Heinekamp T, Dahse H-M, Schmaler-Ripcke J, Nietzsche S, Zipfel PF, Brakhage AA. 2011. Conidial dihydroxynaphthalene melanin of the human pathogenic fungus Aspergillus fumigatus interferes with the host endocytosis pathway. Front Microbiol 2:96. https://doi.org/10.3389/fmicb.2011.00096.

15. Silva JC, Rodrigues NC, Thompson-Souza GA, Muniz VS, Neves JS, Figueiredo RT. 2020. Mac-1 triggers neutrophil DNA extracellular trap formation to Aspergillus fumigatus independently of PAD4 histone citrullination. J Leukoc Biol 107:69–83. https://doi.org/10.1002/JLB.4A0119-009RR.

16. Bruns S, Kniemeyer O, Hasenberg M, Aimanianda V, Nietzsche S, Thywissen A, Jeron A, Latge JP, Brakhage AA, Gunzer M. 2010. Production of extracellular traps against Aspergillus fumigatus in vitro and in infected lung tissue is dependent on invading neutrophils and influenced by hydrophobin RodA. PLoS Pathog 6:e1000873. https://doi.org/10.1371/journal.ppat.1000873.

17. Clark HL, Abbondante S, Minns MS, Greenberg EN, Sun Y, Pearlman E. 2018. Protein deiminase 4 and CR3 regulate Aspergillus fumigatus and beta-glucan-induced neutrophil extracellular trap formation, but hyphal killing is dependent only on CR3. Front Immunol 9:1182. https://doi.org/10.3389/fimmu.2018.01182.

18. Zarember KA, Sugui JA, Chang YC, Kwon-Chung KJ, Gallin Jl. 2007. Human polymorphonuclear leukocytes inhibit Aspergillus fumigatus conidial growth by lactoferrin-mediated iron depletion. J Immunol 178:6367–6373. https://doi.org/10.4049/jimmunol.178.10.6367.

19. Gazendam RP, van Hamme JL, Tool AT, Hoogenboezem M, van den Berg JM, Prins JM, Vitkov L, van de Veerdonk FL, van den Berg TK, Roos D, Kuijpers TW. 2016. Human neutrophils use different mechanisms to kill Aspergillus fumigatus conidia and hyphae: evidence from phagocyte defects. J Immunol 196:1272–1283. https://doi.org/10.4049/jimmunol.1501811.

20. Lahoz-Beneytez J, Elemans M, Zhang Y, Ahmed R, Salam A, Block M, Niederalt C, Asquith B, Macallan D. 2016. Human neutrophil kinetics: modeling of stable isotope labeling data supports short blood neutrophil half-lives. Blood 127:3431–3438. https://doi.org/10.1182/blood-2016-03-700336.

21. Blanter M, Gouwy M, Struyf S. 2021. Studying neutrophil function in vitro: cell models and environmental factors. J Inflamm Res 14:141–162. https://doi.org/10.2147/JIR.S284941.

22. Marin-Esteban V, Turbica I, Dufour G, Semiramoth N, Gleizes A, Gorges R, Beau I, Servin AL, Lievin-Le Moal V, Sandre C, Chollet-Martin S. 2012. Afa/Dr diffusely adhering Escherichia coli strain C1845 induces neutrophil extracellular traps that kill bacteria and damage human enterocyte-like cells. Infect Immun 80:1891–1899. https://doi.org/10.1128/IAI.00050-12.

23. Amulic B, Knackstedt SL, Abu Abed U, Deigendesch N, Harbort CJ, Caffrey BE, Brinkmann V, Heppner FL, Hinds PW, Zychlinsky A. 2017. Cell-cycle proteins control production of neutrophil extracellular traps. Dev Cell 43:449–462.e5. https://doi.org/10.1016/j.devcel.2017.10.013.

24. Baistrocchi SR, Lee MJ, Lehoux M, Ralph B, Snarr BD, Robitaille R, Sheppard DC. 2017. Posaconazole-loaded leukocytes as a novel treatment strategy targeting invasive pulmonary aspergillosis. J Infect Dis 215:1734–1741. https://doi.org/10.1093/infdis/jiw513.

25. Braem SG, Rooijakkers SH, van Kessel KP, de Cock H, Wosten HA, van Strijp JA, Haas PJ. 2015. Effective neutrophil phagocytosis of Aspergillus fumigatus is mediated by classical pathway complement activation. J Innate Immun 7:364–374. https://doi.org/10.1159/000369493.

26. Goyette G, Boulais J, Carruthers NJ, Landry CR, Jutras I, Duclos S, Dermine JF, Michnick SW, LaBoissiere S, Lajoie G, Barreiro L, Thibault P, Desjardins M. 2012. Proteomic characterization of phagosomal membrane microdomains during phagolysosome biogenesis and evolution. Mol Cell Proteomics 11:1365–1377. https://doi.org/10.1074/mcp.M112.021048.

27. Heinekamp T, Schmidt H, Lapp K, Pahtz V, Shopova I, Koster-Eiserfunke N, Kruger T, Kniemeyer O, Brakhage AA. 2015. Interference of Aspergillus fumigatus with the immune response. Semin Immunopathol 37:141–152. https://doi.org/10.1007/s00281-014-0465-1.

28. Schmidt F, Thywißen A, Goldmann M, Cunha C, Cseresnyés Z, Schmidt H, Rafiq M, Galiani S, Gräler MH, Chamilos G, Lacerda JF, Campos A, Eggeling C, Figge MT, Heinekamp T, Filler SG, Carvalho A, Brakhage AA. 2020. Flotillin-dependent membrane microdomains are required for functional phagolysosomes against fungal infections. Cell Rep 32:108017. https://doi.org/10.1016/j.celrep.2020.108017.

29. Pedruzzi E, Fay M, Elbim C, Gaudry M, Gougerot-Pocidalo MA. 2002. Differentiation of PLB-985 myeloid cells into mature neutrophils, shown by degranulation of terminally differentiated compartments in response to N-formyl peptide and priming of superoxide anion production by granulocyte-macrophage colony-stimulating factor. Br J Haematol 117:719–726. https://doi.org/10.1046/j.1365-2141.2002.03521.x.

30. Volk AP, Barber BM, Goss KL, Ruff JG, Heise CK, Hook JS, Moreland JG. 2011. Priming of neutrophils and differentiated PLB-985 cells by pathophysiological concentrations of TNF-alpha is partially oxygen dependent. J Innate Immun 3:298–314. https://doi.org/10.1159/000321439.

31. Branzk N, Papayannopoulos V. 2013. Molecular mechanisms regulating NETosis in infection and disease. Semin Immunopathol 35:513–530. https://doi.org/10.1007/s00281-013-0384-6.

32. Xie K, Varatnitskaya M, Maghnouj A, Bader V, Winklhofer KF, Hahn S, Leichert LI. 2020. Activation leads to a significant shift in the intracellular redox homeostasis of neutrophil-like cells. Redox Biol 28:101344. https://doi.org/10.1016/j.redox.2019.101344.

33. Timar CI, Lorincz AM, Csepanyi-Komi R, Valyi-Nagy A, Nagy G, Buzas EI, Ivanyi Z, Kittel A, Powell DW, McLeish KR, Ligeti E. 2013. Antibacterial effect of microvesicles released from human neutrophilic granulocytes. Blood 121:510–518. https://doi.org/10.1182/blood-2012-05-431114.

34. Brakhage AA, Zimmermann A-K, Rivieccio F, Visser C, Blango MG. 2021. Host-derived extracellular vesicles for antimicrobial defense. microLife 2: uqab003. https://doi.org/10.1093/femsml/uqab003.

35. Lane RE, Korbie D, Trau M, Hill MM. 2019. Optimizing size exclusion chromatography for extracellular vesicle enrichment and proteomic analysis from clinically relevant samples. Proteomics 19:e1800156. https://doi.org/10.1002/pmic.201800156.

36. Ruf D, Brantl V, Wagener J. 2018. Mitochondrial fragmentation in *Aspergillus fumigatus* as early marker of granulocyte killing activity. Front Cell Infect Microbiol 8:128. https://doi.org/10.3389/fcimb.2018.00128.

37. Feldmesser M. 2006. Role of neutrophils in invasive aspergillosis. Infect Immun 74:6514–6516. https://doi.org/10.1128/IAI.01551-06.

38. Pivot-Pajot C, Chouinard FC, El Azreq MA, Harbour D, Bourgoin SG. 2010. Characterisation of degranulation and phagocytic capacity of a human neutrophilic cellular model, PLB-985 cells. Immunobiology 215:38–52. https://doi.org/10.1016/j.imbio.2009.01.007.

39. Bidula S, Sexton DW, Schelenz S. 2016. Serum opsonin ficolin-A enhances host-fungal interactions and modulates cytokine expression from human monocyte-derived macrophages and neutrophils following *Aspergillus fumigatus* challenge. Med Microbiol Immunol 205:133–142. https://doi.org/10.1007/s00430-015-0435-9.

40. Buzas EI, Toth EA, Sodar BW, Szabo-Taylor KE. 2018. Molecular interactions at the surface of extracellular vesicles. Semin Immunopathol 40: 453–464. https://doi.org/10.1007/s00281-018-0682-0.

41. Perez-Hernandez J, Redon J, Cortes R. 2017. Extracellular vesicles as therapeutic agents in systemic lupus erythematosus. Int J Mol Sci 18:717. https://doi.org/10.3390/ijms18040717.

42. Cai Q, Qiao L, Wang M, He B, Lin FM, Palmquist J, Huang SD, Jin H. 2018. Plants send small RNAs in extracellular vesicles to fungal pathogen to silence virulence genes. Science 360:1126–1129. https://doi.org/10.1126/science.aar4142.

43. He B, Cai Q, Qiao L, Huang C-Y, Wang S, Miao W, Ha T, Wang Y, Jin H. 2021. RNA-binding proteins contribute to small RNA loading in plant extracellular vesicles. Nat Plants 7:342–352. doi:10.1038/s41477-021–00863-8. https://doi.org/10.1038/s41477-021-00863-8.

44. Klebanoff SJ, Kettle AJ, Rosen H, Winterbourn CC, Nauseef WM. 2013. Myeloperoxidase: a front-line defender against phagocytosed microorganisms. J Leukoc Biol 93:185–198. https://doi.org/10.1189/jlb.0712349.

45. Hess C, Sadallah S, Hefti A, Landmann R, Schifferli JA. 1999. Ectosomes released by human neutrophils are specialized functional units. J Immunol 163:4564–4573.

46. Desai JV, Lionakis MS. 2018. The role of neutrophils in host defense against invasive fungal infections. Curr Clin Microbiol Rep 5:181–189. https://doi.org/10.1007/s40588-018-0098-6.

47. Edgar JR. 2016. Q&A: what are exosomes, exactly? BMC Biol 14:46. https://doi.org/10.1186/s12915-016-0268-z.

48. Hillmann F, Novohradska S, Mattern DJ, Forberger T, Heinekamp T, Westermann M, Winckler T, Brakhage AA. 2015. Virulence determinants of the human pathogenic fungus *Aspergillus fumigatus* protect against soil amoeba predation. Environ Microbiol 17:2858–2869. https://doi.org/10.1111/1462-2920.12808.

49. Kraibooj K, Schoeler H, Svensson CM, Brakhage AA, Figge MT. 2015. Automated quantification of the phagocytosis of *Aspergillus fumigatus* conidia by a novel image analysis algorithm. Front Microbiol 6:549. https://doi.org/10.3389/fmicb.2015.00549.

50. Wessel D, Flügge UI. 1984. A method for the quantitative recovery of protein in dilute solution in the presence of detergents and lipids. Anal Biochem 138:141–143. https://doi.org/10.1016/0003-2697(84)90782-6.

51. Lex A, Gehlenborg N, Strobelt H, Vuillemot R, Pfister H. 2014. UpSet: visualization of intersecting sets. IEEE Trans Vis Comput Graph 20:1983–1992. https://doi.org/10.1109/TVCG.2014.2346248.

52. Perez-Riverol Y, Xu QW, Wang R, Uszkoreit J, Griss J, Sanchez A, Reisinger F, Csordas A, Ternent T, Del-Toro N, Dianes JA, Eisenacher M, Hermjakob H, Vizcaino JA. 2016. PRIDE Inspector Toolsuite: moving toward a universal visualization tool for proteomics data standard formats and quality assessment of ProteomeXchange datasets. Mol Cell Proteomics 15: 305–317. https://doi.org/10.1074/mcp.O115.050229.